AIAA

AIAA 98-0164

Heat and Mass Transfer for Isolated and Interacting Fluid Drops Under Quiescent Supercritical Conditions

K. Harstad and J. Bellan
Jet Propulsion Laboratory
Pasadena, CA

36th Aerospace Sciences
Meeting & Exhibit
January 12-15, 1998 / Reno, NV

HEAT AND MASS TRANSFER FOR ISOLATED AND INTERACTING FLUID DROPS UNDER SUPERCRITICAL CONDITIONS[1]

K. Harstad and J. Bellan
Jet Propulsion Laboratory
California Institute of Technology
4800 Oak Grove Drive
Pasadena, CA. 91109

Abstract

A model has been developed for the behavior of an isolated fluid drop of a single component species immersed into another single component species in finite, quiescent surroundings at supercritical conditions. The model is based upon fluctuation theory which accounts for both Soret and Dufour effects in the calculation of the transport matrix relating molar and heat fluxes to the transport properties and the thermodynamic variables. The contribution of the chemical potentials to the fluxes is fully included and accounts for potentially non-unity mass diffusion factors and transport effects of enthalpy and molar volumes with temperature gradients and pressure gradients, respectively. This model has been used as a building block in a formulation describing interactions of fluid drops induced by drop proximity. Heat and mass transfer to the cluster are modeled using the Nusselt number concept. Calculations were performed for the LO_x -- H_2 system; the transport properties have been modeled over a wide range of pressure and temperature variation applicable to LO_2 -- H_2 conditions in rocket engine combustion chambers, and the equations of state have been calculated using a previously-derived, computationally-efficient and accurate protocol. The results show that the supercritical behavior is essentially one of diffusion. The temperature profile relaxes fastest followed by the density and lastly by the mass fraction profile. To understand heat and mass transfer, an effective Lewis number was calculated for situations where temperature and mass fractions gradients are very large. Results show that the effective Lewis number can be 2 to 40 times larger than the traditional Lewis number and that the spatial variation of the two numbers is different; the reason for these Lewis number effects is discussed. Parametric simulations as a function of pressure show that length scales decrease with increasing pressure. This hinders interdiffusion for isolated fluid drops, but enhances it for clusters of drops due to the additional effect of increasing cluster volume.

Introduction

Liquid rocket engine design is not a mature technology in that the issues of reliability and efficiency are unresolved. Current designs are still based upon empirical knowledge and theory that does not portray the complexities of the physical processes and of the environment in the combustion chambers. The extensive review on liquid propellant rocket instabilities compiled by Harrje and Reardon [1] more than twenty years ago remains the base of rocket design despite the increased understanding that many of the approximations made in performing the calculations compromise the validity of the results.

One of the foundations of liquid rocket instabilities is the theory of isolated drop evaporation and combustion in an infinite medium [I], [2]. The early version of that theory was based on the assumption of quasi-steady gas behavior with respect to the liquid phase, an assumption strictly valid only at low pressures where the liquid density is three orders of magnitude larger than that of the gas. Recognizing that at the elevated pressures of liquid rocket chambers the liquid density approaches that of the gas, the quasi-steady assumption was relaxed in other investigations [3], [4], [5], [6], [7]. However, it is only recently that the description of the full complexity of combustion chambers processes was sought; this includes not only the complete unsteady treatment of the conservation equations but also appropriate equations of state with consistent mixing rules and transport properties valid over transcritical/supercritical conditions. Recent studies related to these aspects are those of Yang et al. [8], Hsiao et al. [9], Delplanque and Sirignano [10] and Haldenwang et al. [11].

Isolated drop behavior, although very relevant to understanding phenomena in rocket engine motors, is by itself insufficient for deriving the necessary insight into controlling liquid rocket combustion operation. Experimental observations of atomization of coaxial jets (such as those used in liquid rocket engines) by Hardalupas et al. [12] and Engelbert et al. [13] reveal the initial formation of ligaments, each ligament quickly disintegrating into a cluster of drops. Similarly, visualizations of impinging liquid jets [I] have shown that un-

der both cold and hot flow conditions the jets break up in a periodic manner into ligaments which further break up into drops thereby creating clusters of drops. Recent observations by Ryan et al. [14] have documented this typical breakup process while also yielding information regarding the breakup length and the drop size for both laminar and turbulent impinging jets. Poulikakos [15] made similar observations.

These observations indicate that fluid drops created during atomization in liquid rocket chambers c1o not behave as isolated and instead have a collective behavior. This realization is very important for controlling high frequency combustion instabilities because the response function must incorporate this fluid drop interaction.

Fluid drop interaction at high pressure has been modeled by Jiang and Chiang [16] using the concept of 'sphere of influence' of Bellan and Cuffel [17] and results were obtained for n-pentane adiabatic drop arrays where the drops are uniformly distributed and stationary. The model of Jiang and Chiang [16] does not include the intricacies of high pressure transport processes, and thus it is not appropriate for the supercritical regime where Fick's and Fourier's laws are 1 1o longer solely able to completely describe the t ransport matrix [18]. Additionally, the interdrop distance might not have similar values under subcritical and supercritical conditions since in the former situation the liquid drops have a motion distinct from that of the surrounding gas whereas in the latter situation, because the densities of the two fluids are more similar, their motion is also more similar. Moreover, the dense spray effects identified at subcritical conditions were the consequence of both high mass and relatively high volume loading; in supercritical conditions, the relatively high volume loading is not necessarily accompanied by high mass loading because of the density ratio effect. This indicates that dense spray effects might be encountered in supercritical conditions only for interdrop distances much smaller than in subcritical conditions. In fact, dense spray effects will visually manifest as small scale density variations, consistent with the discussed observations for coaxial and impinging jets atomization [12], [13], [14] and [15].

This study is devoted to both establishing, from first principles, a set of conservat ion equations describing isolated fluid drop behavior and to establishing a model of fluid drop interactions. These models constitute the frame work for identifying the major differences in behavior between that known for liquid drops at subcritical conditions and that found here for fluid drops under supercritical conditions.

Model

The model of the conservation equations for the isolated fluid drop is based on the fluctuation theory of Keizer [19], also described by Peacock-Lopez and Woodhouse [20]. The advantage of this theory is that it inherently accounts for nonequilibrium processes and naturally leads to the most general fluid equations by relating the partial molar fluxes, $\vec{J}_i$, and the heat flux, $\vec{q}$, to thermodynamic quantities. These equations have been derived in detail in Harstad and Bellan [18], and therefore it is only a brief description that will be provided here.

Fluctuation theory relates $\vec{J}_i$ and $\vec{q}$ to the transport matrix L through

$$\vec{J}_i = L_{iq}\nabla\beta - \sum_{j=1}^{\mathcal{N}} L_{ij}\nabla(\beta\mu_j), \quad \vec{q} = L_{qq}\nabla\beta - \sum_{j=1}^{\mathcal{N}} L_{qj}\nabla(\beta\mu_j) \tag{1}$$

Here L_{ij} are the Fick's diffusion elements, L_{qq} is the Fourier thermal diffusion element, L_{iq} are the Soret diffusion and L_{qj} are the Dufour diffusion elements, μ_j is a chemical potential and $\beta \equiv 1/(R_u T)$ where T is the temperature and R_u is the universal gas constant. The Onsager relations state that $L_{ij} = L_{ji}$ and $L_{iq} = L_{qi}$. Additionally, conservation of fluxes and mass in the system imply that $\sum_i^{\mathcal{N}} m_i \vec{J}_i = \vec{0}$ and $\sum_i^{\mathcal{N}} L_{ij} m_i = 0$ for $j \in [1, \mathcal{N}]$ and j = g, where m_i are the molar masses.

Using the thermodynamic relationship

$$d(\beta\mu_j) = \beta(v_j dp - h_j d\ln T) + \Big(\sum_{i=1}^{\mathcal{N}-1} \alpha_{Dji} dX_i\Big)/X_j \tag{2}$$

where

$$\alpha_{Dij} \equiv \beta X_i \partial\mu_i/\partial X_j = \partial X_i/\partial X_j + X_i \partial \ln\gamma_i/\partial X_j \tag{3}$$

are the mass diffusion factors, one can calculate $\vec{J}_i$ from Eqs. 1 and 2. Here v_j are the partial molar volumes, p is the pressure, h_j are the molar enthalpies, γ_i are the activity coefficients and X_i are the molar fractions. This formalism proceeds with the definition of a symmetric matrix whose elements are the pair-wise mass diffusion coefficients for the mixture $D_{mix}^{(ij)}$, and an antisymmetric matrix whose elements are the thermal diffusion factors $\alpha_T^{(ij)}$. The main result is that the transport matrix has the following form:

$$\begin{aligned} J &= \textstyle\sum_j A_{J,j}\,\nabla Y_j + B_J\nabla T + C_J\nabla p' \\ q &= A_q\nabla T + \textstyle\sum_j C_{q,j}\,\nabla Y_j + B_q\nabla p \end{aligned} \tag{4}$$

where p' is the dynamic pressure, and the A's, B's and C's are functions of the dependent variables. The terms proportional to the gradient of the dynamic pressure in the expressions for J and q will be neglected in the following because that gradient is proportional to Ma^2, where Ma is the Mach number, and $Ma \ll 1$; while coefficients C_J and B_q are no larger than other coefficients in the equations. Spatial variations of p' were

confirmed to be small by results from calculations of isolated entities of LO_x in fluid H_2 at high pressures [18].

To obtain the system of conservation equations, the flux mat rix is used into the Navier-Stokes equations. Within this self consistent derivation, the thermodynamically related transport coefficients are naturally defined: $D_m^{(ij)} = -L_{ij}(m^2/m_i m_j)v/(X_i X_j)$ are the mass diffusion coefficients (m is the molar mass and v is the molar volume) and $\lambda = \beta L_{qq}/T$ is the thermal conductivity. Also, the ratios between the thermal and mass diffusivities $\alpha_T^{(ij)}$ are related to the mass diffusion coefficients and the elements of the transport matrix through $\beta m v L_{iq}/X_i = \sum_{j \neq i} m_j X_j \alpha_T^{(ij)} D_m^{(ij)}$.

The general form of the flux matrix indicates that even in the simplified case when there are only two single-component substances, which is the focus of this study, the traditional calculation of the Lewis number, $Le \equiv D_T/D_m = \lambda/(\rho C_p D_m)$, may not be appropriate for a general fluid (D_T is the thermal diffusivity and D_m is the mass diffusivity). This is because even if there is only one diffusion coefficient, the characteristic length scales for heat and mass transfer are no longer given by the multiplying factors of the Fourier and Fick's diffusion terms. In fact, due to the general form of the flux matrix, these scales are not immediately apparent and additional analysis is necessary to find them. Harstad and Bellan [21] present such au analysis that leads to the Lewis number calculation from a general form, $Le_{eff} = \lambda_{eff}/(\rho C_p D_{eff})$. The analysis is valid under the assumptions of quasi-steadiness, large gradients, and large emission rates from the fluid drop. The final result of the detailed analysis is that λ_{eff} contains an additional, positive contribution with respect to λ, whereas D_{eff} is reduced by a negative contribution with respect to D_m. The results presented below will emphasize the impact of these findings.

Finally, the model for the cluster of drops is obtained by coupling the isolated fluid drop equations with a set of conservation equations for the entire cluster. The derivation has been described in detail in Harstad and Bellan [22], and it is only the fundamental concept is discussed here: Whereas the isolated fluid drop equations are solved in a finite domain where the far field boundary is located at a distance that changes as a function of time due to processes related to that sphere of influence, for interacting drops this distance changes as a function of processes in all spheres of influence and is a solution of the cluster conservation equations. In the same manner, whereas the far field values of the dependent variables are prescribed for the isolated fluid drop, for interacting drops they are found as a function of time from the solution of the global cluster conservation equations.

Boundary Conditions

For spherical drops, boundary conditions arc applied at three different locations for the isolated fluid drop: the drop center, the interface separating initially the two pure substances, ancl the far field; for the cluster, an additional boundary condition is imposed at the cluster boundary with its surroundings.

At the center of each fluid drop, spherical symmetry conditions prevail, whereas at the edge of the sphere of influence the dependent variables are prescribed.

The conditions at the interface express not only conservation of mass, species, momentum and energy, but also nonequilibrium evaporation (when applicable) and solvation. Initially, the fluid drop exists for r < R_d and at $t = 0$, a predominantly different fluid surrounds the drop ($r > R_d$). In cent rast to the purely subcritical situation [17] where the interface is well defined by a surface where there is a sharp change in density, here there is an arbitrariness in defining an interface that should be followed in time. As we show in the Results section, the gradients of the mass fraction and density do not coincide, so that following the pure drop interface is not equivalent to following the maximum density gradient, which is what is optically detected. Since at supercritical conditions the physical phase change interface does not exist, we are free to choose an interface that we want to follow; by choice, here we follow the interface of the initially pure fluid drop.

For a spherical cluster, the gradients at the cluster boundary may be approximated by a difference across an external length scale, r-$_e$, which is related to what is equivalent to a Nusselt number, Nu_C, by $r_e = R_C/Nu_C$, where R_C is the cluster radius. *A priori*, the assumption was made that r_e is the same for heat and mass transfer, although the results found below show that the mass transfer scales are larger than those for heat transfer. However, there was no previous information leading to appropriate heat and mass transfer length scales, and thus it did not seem justifiable to make an ad hoc assumption about their ratio. To study the impact of transport to the cluster, parametric simulations were performed [22] with Nusselt numbers over the range $10^2 - 10^5$ and it was found that the variation in the results was minimal; this is due to heat transfer from the cluster interstitial region to the drops being much faster than that from the surroundings to the cluster.

Equations of State and Transport Properties

The actuations of state (EOS) were calculated according to the procedure described in Harstad et al. [23] in order to extend the experimentally derived EOS'S beyond the range of the data and also to obtain analytic forms suitable to using mixing rules.

The calculation of viscosities, thermal conductivities and diffusivities is described in detail in Harstad

and Bellan [18]. Essentially, for each put-c substante, both viscosities and thermal conductivities are calculated using a protocol whereby it is first the low p limit that is correlated, then this function is subtracted from the high p data to create an excess function, and finally the high p data is correlated. The corresponding states formalism of Teja and Rice [24] is used to calculate the mixture properties.

The diffusion coefficients are calculated in four steps [18]: (1) binary infinite dilution diffusion coefficients for a gas, (2) infinite dilution diffusion coefficients for a liquid, (3) infinite dilution coefficients for a fluid under general conditions, and (4) binary diffusion coefficients using the corresponding states formalism of Teja and Rice [24].

Results

The results presented here are for the $LO_x - H_2$ system for which the critical conditions are the following: T_c is 154.6 K and 33.2 K respectively and p_c is 5.043 MPa and 1.313 MPa respectively. Table 1 contains a summary of the initial conditions used in the simulations; N is the number of drops in the cluster ($N = 1$ represents the isolated drop). For isolated drops, the pressure and temperature at the edge of the sphere of influence (the far field; subscript si) are constant during the calculation. For clusters of drops, the initial interstitial temperature and pressure is always that of the cluster surroundings, but the interstitial values are functions of time according to the global, cluster conservation equations. Other initial conditions used are: fluid drop radius of 50x 10^{-4} cm, fluid drop temperature of 100 K and fluid hydrogen temperature of 1000 K.

The presentation of the results is organized as follows: First a baseline behavior of the isolated fluid drop is discussed. Then a baseline cluster behavior is analyzed for the same initial conditions; a study of the fluid drop interaction follows as the initial radius of the sphere of influence is varied. Finally, we explore the influence of the pressure on both isolated ancf interacting drops.

Baseline behavior of isolated drops

Run 2 represents the baseline situation whose results are illustrated in Fig. 1 where the spatial variation of T, ρ and Y_i ($i = 1$ refers to LO_x) is shown as a function of time. Comparisons between the variation of these quantities show that the density gradient is the steepest, however it does not remain steep during the entire time necessary for drop heating. It is this density gradient that is captured in optical measurements; since the gradient eventually relaxes, the optical measurement yields increasingly uncertain results as t increases. Also, the density gradient does not correspond to the Y_i gradient indicating that it is not the evolution of the pure LO_x fluid drop that is followed in the measurements, but that of an entity into which hydrogen has diffused. The pure LO_x fluid drop shrinks very fast and eventually disappears as shown in Fig. 1 by $Y_1(r = 0) < 1$. It is important to realize that not only c1o gradients of Y_1 anti T occur at different locations, but also that early-time gradients of T are steeper than gradients of Y_i whereas at later time the opposite is true. The relaxation of the T and p profiles occurs much faster than that of Y_i because D_T is considerably larger than D_m as shown by their ratio, the traditional Le plotted in Fig. 2. Moreover, the effective Lewis number, Le_{eff}, also illustrated in Fig.2, is about a factor of 40 larger than the traditional Le indicating that the ratio of heat to mass diffusion is even larger than indicated by Le. Comparisons between our results and those of Yang et al. [8] for Le shows that we predict similar Le variations, although our values are huger for a given pressure, as will be discussed in the parametric variations below.

The spatial variation of Le_{eff} is essentially different of that of Le in that it is nonmonotonic even after the memory of the initial condition is lost. This is because Le_{eff} implicitly accounts for Y_i and T gradients effects; these Y_i and T gradients do not occur at the same location under supercritical conditions. Thus, the spatial variation of Le_{eff} is directly related to the variation of Y_i and T gradients as follows: For small r, the shallow part of the curves corresponds mostly to the large $\partial T/\partial r$, Y_i being mostly uniform, and the temporal increase of Le_{ff} is due to the increased T. The strongly increasing branch of Le_{eff} corresponds to the region of large $\partial Y_1/\partial r$ and the location of the maximum Le_{eff} is directly related to the maximum Y_1 gradient. Finally, the decreasing part of the Le_{eff} curves corresponds to the decreasing $\partial Y_1/\partial r$ and the asymptotic leveling of T. In contrast, the Le spatial variation reflects only the dependence of D_T and D_m upon composition and T.

Parametric studies with various values of the thermal diffusion factors (0.0, 0.01 and 0.05) show no sensitivity of the results to Soret and Dufour effects for the $LO_x - H_2$ system. The difference between Le and Le_{eff} is due to the combined effect of the contribution of the chemical potentials to the fluxes through a small mass diffusion factor and transport effects of enthalpy with temperature gradients.

Clusters of drops behavior

As discussed above, due to the essentially diffusive behavior at high pressure it is expected that dense spray effects will be important only for fluid-drops in closer proximity than in subcritical conditions; therefore, $R^0_{si} = 2R^0_d$ is chosen as a baseline behavior. Figure 3 illustrates the spatial profiles of T, Y_1 and ρ at different times while Fig. 4 depicts the time evolution of $T_{si}, Y_{1,si}, \rho_{si}$, N_d (drop number density), R_{si} and

R_C. Comparisons between the calculated baseline results and those obtained for $R^0_{si} = 5R^0_d$ and $R^0_{si} = 10R^0_d$ (see that the results fOr Runs 8 and 2 arc essentially the same) under otherwise identical conditions are presented in Fig. 5. While the baseline spatial variation of T, Y_1 and ρ parallels that obtained for the isolated drop in that it is mainly a diffusion process, the closer drop proximity induces smaller density gradients (Fig. 5c), steeper Y_1 gradients (Fig. 5b) and larger temperatures as the initial interstitial temperature is equal to that of the cluster surroundings. An important difference among the results obtained with decreasing R^0_{si}/R^0_d is the increased accumulation of a non-negligible amount of LO_2 in the interstitial region (see Fig. 4a) as the cluster contracts due to heat being transferred faster from the interstitial region to the fluid LO_x drops than it is replenished from the cluster surroundings. This is consistent with the small decrease of T_{si}, R_{si} and R_C and the equivalent increase in ρ_{si} shown in Fig. 4. Eventually, T_{si} increases due to the increased amount of heat transferred to the cluster from its surroundings, and $Y_{1,si}$ accordingly decreases. All these effects are small for the values used in this baseline calculation; in particular, the value of Nu_C is too small for heat transfer from the cluster surroundings to replenish the heat relinquished by the interstitial fluid to the fluid drops. In fact, just as in subcritical cluster studies [25], the motion of the cluster boundary is governed by the ratio of two characteristic times: that of heat transferred from the interstitial region to the drops (a heat sink), t_1, and that transferred from the cluster surroundings to the cluster (a heat source), t_2; the only difference with the subcritical studies is the absence of phase change which requires a substantial heat budget. The latent heat carried away by the evaporated compound in subcritical situations constitutes a major percentage of the heat input to the gas phase. This explains the present, relatively undramatic cluster contraction and expansion. However, results from calculations with Nu_C in the range 10^3 to 105 show a surprising insensitivity to the value of Nu_C [22]. This results is plausibly due to the combined effects of: (1) the value of r_e for mass and heat transfer being taken identical, whereas Le_{eff} suggests that it should be considerably larger for mass transfer, and (2) the modeling of transfer across the cluster boundary using an equivalent Nusselt number being somewhat uncertain.

The effect of pressure

In Fig. 6 we display results for fixed initial drop size and surrounding temperature as a function of surrounding pressure at 2 x 10^{-2} s. The slightly larger λ but much larger C_p with increasing p on the LO_2 side of the interface (not shown) result in smaller Ton the LO_x side of the interface; the opposite occurs on the H_2 side of the interface. Thus, T gradients are greater with increasing p, Increasing the surrounding p decreases both D_m and D_T (not shown); however, there is relatively a larger reduction on the H_2 side of the interface. The decrease in D_m explains the smaller Y_1 on the H_2 side of the interface and the steeper gradients with increasing p. Examination of the p profiles shows the considerably larger gradients with increasing p; it is thus inferred that experiments quantifying the interface motion will be more accurate when performed at large pressures. Examination of the variation of Le with increasing p [21] shows that as p increases, Le remains <1 on the LO_x side of the interface, and decreases with increasing p, whereas Le remains > 1 on the H_2 side of the interface and increases with increasing p [21]; the Lewis number seems insensitive to the pressure in the far field. This spatial variation with increasing p shows that indeed the gradients become steeper with increasing p.

The general variation of the dependent variables with increasing p for isolated fluid drops indicates that since the gradients become larger due to a reduction in scales, high pressure combustion in practical devices will have to rely on strong turbulence to enhance mixing and heat transfer.

To investigate the impact of drop interactions with surrounding pressure, extensive calculations were performed by varying the surrounding cluster pressure from 10 MPa to 80 MPa. The results at 10^{-2} s are depicted in Fig. 7. Unlike in the isolated drop situation where gradients were greater with increasing pressure, here it is exactly the opposite. The effect of the drop interaction is to smear the gradients by increasing the cluster volume with increasing pressure. This volume increase is a direct consequence of the reduction in ρC_p with increasing pressure in the predominantly-LO_x side of the interface; this results in a temperature augmentation in this region, which increases the average cluster temperature, and thus its volume. A more minor effect, which increases the available heat source, is the slight elevation of the interstitial molar enthalpy with increasing pressure. Thus, the presence of clusters of drops in burning sprays tends to render the dependent variables more uniform with increasing pressure whereas the opposite is true for isolated drops. In this respect, clusters of drops are a desirable aspect because they aid the interdiffusion of the reactive components.

Conclusions

A model of an isolated fluid drop in quiescent, finite spatial surroundings has been derived using the formalism of fluctuation theory. The model presented here is derived from first principles and incorporates all physical aspects of high pressure behavior including Soret and Dufour effects, high pressure mixture-thermodynamics and mixture transport properties over a wide range of pressures and temperatures. This model has been further used as a building block for a more general fluid drop cluster model wherein it was coupled to global conservation equations derived for the entire cluster.

Since the transport matrix is no longer composed of the Fick and Fourier terms which form the basis of the traditional Lewis number calculation, an effective Lewis number has been calculated based upon the results of a simplified analysis that retains the Soret and Dufour contributions, and includes the effects of the mass diffusion factors as well as transport effects of enthalpy and molar volumes with temperature gradients and pressure gradients, respectively.

Results obtained for the $LO_x - H_2$ system show that the supercritical behavior is that of a slow diffusion process. The spatial temperature profile is the first to relax, followed by the density profile; the mass fractions remain nonuniform long after relaxation of both temperature and density. Given the long characteristic time associated with diffusion, it is not surprising that strong turbulence is needed to mix LO_x and H_2 in liquid rocket engines.

Parametric studies performed for the $LO_x - H_2$ system for various drop proximities show that the most important cluster effect is the accumulation of a non-negligible amount of LO_x with decreasing drop interdistance. The effect of drop proximity decreases with increasing pressure in that the behavior of the fluid drops in a very dense gas becomes increasingly similar to a pure diffusion process. For given initial drop proximity, an increase in pressure results in increased smearing of the gradients, a desirable aspect because it promotes interdiffusion. This result is exactly the opposite of what is obtained for isolated fluid drops.

Calculations of the effective Lewis number show that it can be larger than the Lewis number by a factor of **40.** Additionally, the traditional Lewis number and effective Lewis number have different spatial variations, indicating that the traditional Lewis number is not even a qualitative measure of the relative importance of heat and mass transfer.

ACKNOWLEDGMENT

This research was conducted at the Jet Propulsion Laboratory under sponsorship from the National Aeronautics and Space Administration, the George C. Marshall Space Flight Center with Mr. Klaus W. Gross as technical contract monitor and from the National Aeronautics and Space Administration, the Lewis Research Center with Drs. Edward Mularz and Daniel L. Bulzan as technical contract monitors. Their continuing interest and support are greatly appreciated.

References

[1] Harrje, D. T. and Reardon, F. H., *Liquid Propellant Rocket Combustion Instability,* NASA SP-194 (1972)

[2] Williams, F. A., *Combustion Theory,* Addison-Wesley (1965)

[3] Chervinsky, A., Transient burning of spherical symmetric fuel droplets, *Isr. J. Technol.* **7**, 66-73 (1969)

[4] Nuruzzaman, A. S. M. and Beer, J. M., On the nonsteady nature of droplet combustion, *Combust. Sci. and Tech. 3,17-24 (1971)*

[5] Matlosz, R. L., Leipziger, S. and Torda, T. P., Investigation of a liquid drop evaporation in a high temperature and high pressure environment, *Int. J. Heat Mass Transfer* 15, 831-852 (1972)

[6] Rosner, D. E. and Chang, W. S., Transient evaporation and combustion of a fuel droplet near its critical temperature, *Combust. Sci.* and *Tech.* 7,145-158 (1973)

[7] Crespo, A. and Linan, A., Unsteady effects in droplet evaporation and combustion, *Combust. Sci. and Tech.* 11,9-18 (1975)

[8] Yang, V., Lin, N. and Shuen, J-S., Vaporization of liquid oxygen (LOX) droplets in supercritical hydrogen environments, *Combust. Sci. and Tech., 97, 247-270 (1994)*

[9] Hsiao, G. C., Yang V. and Shuen, J. S., Supercritical vaporization and dynamics of liquid oxygen (LOX) droplet in hydrogen stream, AIAA 95-0383, 33rd Aerospace Sciences Meeting, Reno, NV (1995)

[10] Delplanque, J-P. and Sirignano, W. A., Numerical, study of the transient vaporization of an oxygen droplet at sub- and super-critical conditions, *Int. J. Heat Mass Transfer,* 36(2), 303-314 (1993)

[11] Haldenwang, P., Nicoli, C. and Daou, J., High pressure vaporization of LOX droplet crossing the critical condition, *Int. J. Heat Mass Transfer, 39(16), 3453-3464 (1996)*

[12] Hardalupas, Y. Liu, C-H., Tsai, R-l?. and Whitelaw, J. H., Coaxial atomization and combustion, *Proc. IUTA M Symp. on Mechanics and Combustion of Droplets and Sprays,* Tainan, Taiwan, R. O. C., 41-73 (1994)

[13] Engelbert, C. Hardalupas, Y. and Whitelaw, J. H., Breakup phenomena in coaxial airblast atomizers, *Proc. R. Sot. Lend.,* **451**, 189-229 (1995)

[14] Ryan, H. M., Anderson, W. E., Pal, S. and Santoro, R. J., Atomization characteristics of impinging liquid jets, *J. Propulsion and Power,* 11(1), 135-145 (1995)

[15] Poulikakos, D., Determination of structure, temperature and concentration of the near injector region of impinging jets using holographic techniques, *Proc. of the A FOSR Contractors Meeting, 275-278 (1993)*

[16] Jiang, T. L. and Chiang, W.-T., Effects of multiple drop interaction on droplet vaporization in subcritical and supercritical pressure environments, *Combust. and Flame*, *97*, 17-34 (1994)

[17] Bellan, J. and Cuffel, R., A theory of non-dilute spray evaporation based upon multiple drop interaction, *Combust. and Flame*, *51* (l), 55-67 (1983)

[18] Harstad, K. and Bellan, J., Isolated fluid oxygen drop behavior in fluid hydrogen at rocket chamber pressures, submitted (1997)

[19] Keizer, J., *Statistical Thermodynamics of Nonequilibrium Processes*, Springler-Verlag, New York (1987)

[20] Peacock-Lopez, E. and Woodhouse, L., Generalized transport theory and its application to binary mixtures, *Fluctuation Theory of Mixtures*, Advances in thermodynamics, Vol. 2, Eds. Matteoli, E. and Mansoori, G. A., Taylor and Francis, 301-333 (1983)

[21] Harstad, K. and Bellan, J., The Lewis number under supercritical conditions, submitted (1997)

[22] Harst ad, K and Bellan, J., Interactions of fluid oxygen drops in fluid hydrogen at rocket chamber pressures, submitted (1997)

[23] Harstad, K. G. , Miller, R. S., and Bellan, J., Efficient high pressure state equations, *A. I. Ch. E. Journal, 43(6), 1605-1610 (1997)*

[24] Reid, R. C., Prausnitz, J. M. and Polling, B. E., The Properties of Gases and Liquids, 4th Edition, McGraw-Hill Book Company (1987)

[25] Harstad, K. and Bellan, J., A model of the evaporation of binary-fuel cluster of drops, *Atomization and Sprays*, 1, 367-388 (1991)

Run	N	R^0_{si}, cm	R^0_C, cm	p^0_{si}, MPa
1	*1*	0.1		10
2	1	0.1		20
3	1	0.1		25
4	1	0.1		40
5	1	0.1		80
6	5.92×10^{6}	100 X10-4	2	20
7	2.36×10^{6}	250×10^{-4}	2	20
8	1.18×10^{6}	500 X10-4	2	20
9	5.92×10^{6}	100 X10-4	2	10
10	5.92×10^{6}	100 X10-4	2	15
11	5.92×10^{6}	100 X10-4	2	25
12	5.92×10^{6}	100 X10-4	2	40
13	5.92×10^{6}	100 X10-4	2	80

Table 1: Initial conditions for the simulations.

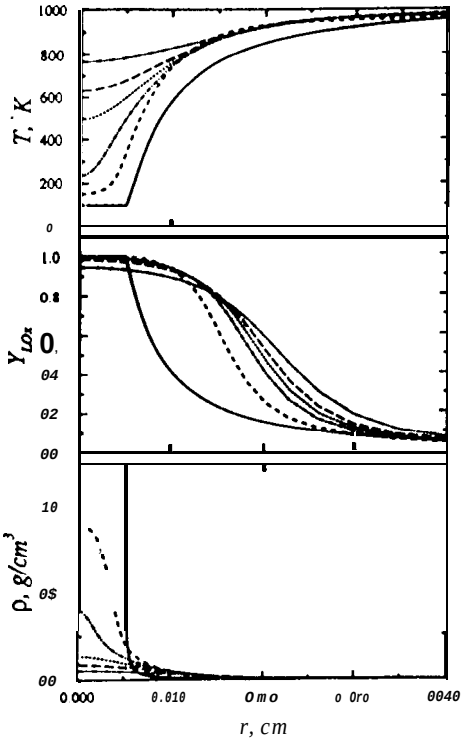

Fig. 1 Spatial variation of the isolated fluid drop temperature, oxygen mass fraction and density at various times for R^0_d = 50 x 10^{-4} cm, R^0_{si} = 0.1 cm, $T^0_{d,b}$ = 100 K , T^0_{si} = *1000* K,and p = 20 MPa. The curves correspond to the following times: 0.0 s (—), 7.5×10^{-3} S (- - -), 1.25×10^{-2} S (– . – ·–·), 1.5×10^{-2} S (· · ·), 1.75×10^{-2} S (–· –), 2.414 x10-2 S (-. ·–).

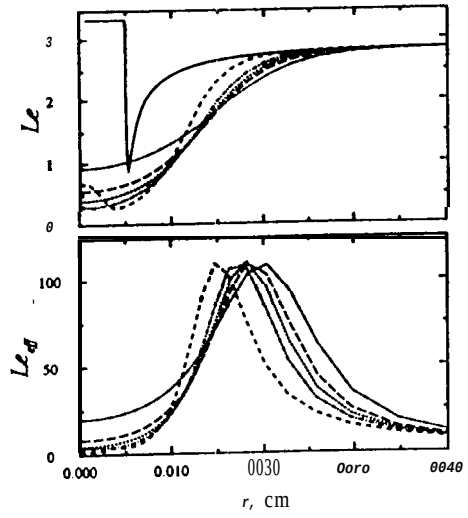

Fig. 2 Spatial variation of the traditional and an effective Lewis number for an isolated fluid drop at different times. The initial conditions are those of Fig. 1 caption.

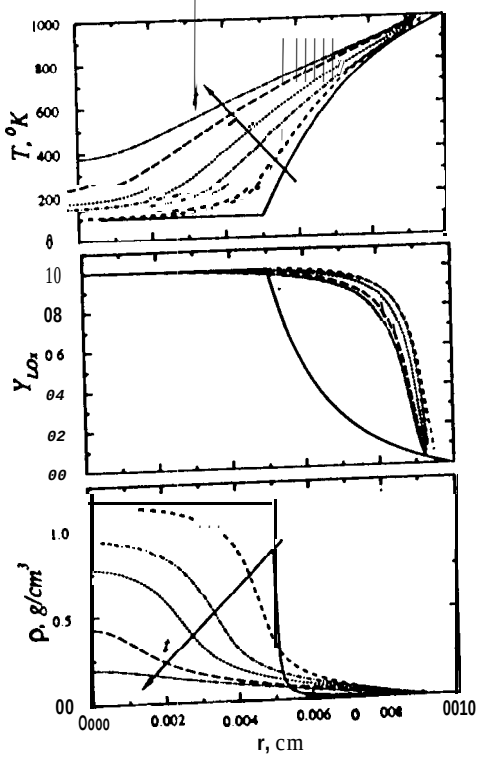

Fig. 3 Spatial variation of the cluster fluid drop temperature (a), oxygen mass fraction (b) and density (c) at various times for $R_d^0 = 50 \times 10^{-4}$ cm, $R_{si}^0 = 2R_d^0$, $R_C^0 = 2$ cm, $T_{db}^0 = 100$K, $Nu_C = 10^2$, $T_{si}^0 = T_e = 1000$ K, $p_e = 20$ MPa and $Y_{1e} = 0$. The curves correspond to the following times: 0.0 s (——), 2X10-³ s (- - -), 6x1 0⁻³ S (– ·—·—), 8x1 0⁻³ S (··· .),1. x10-2 s (———), 1.08 X10-2 s (“ ·—).

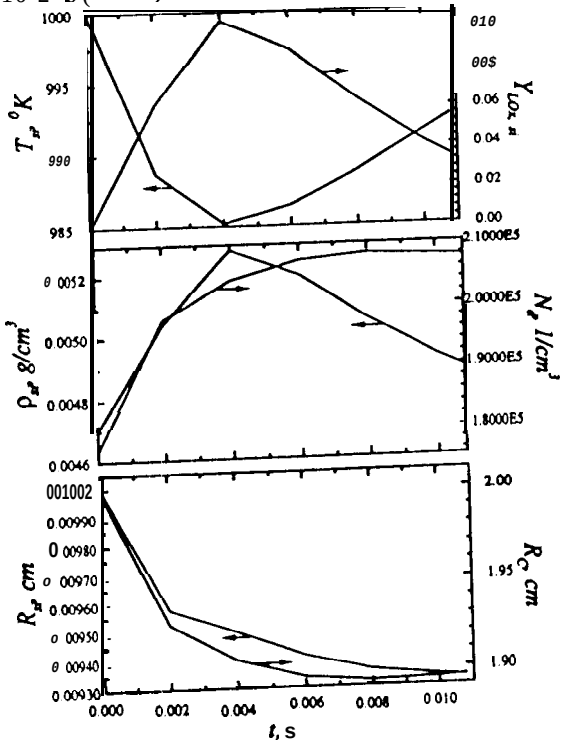

Fig. 4 Time evolution of T_{si} and $Y_{1,si}$ (a), ρ_{si} and N_d (b), and R_{si} and R_C (c) for the same initial conditions as those in Fig. 3 caption.

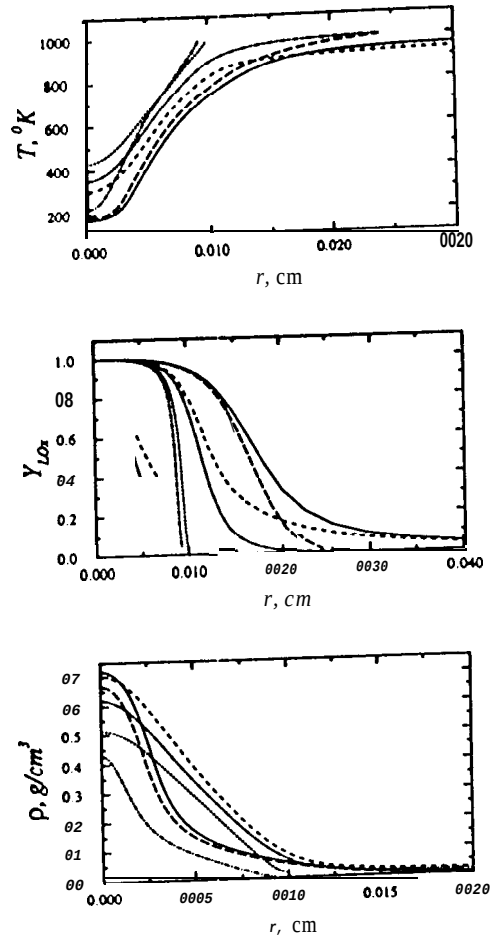

Fig. 5 Spatial variation of the cluster fluid drop temperature (a), oxygen mass fraction (b) and density (.) at $t = 10^{-2}$ s for $R_{si}^0 = 10R_d^0$ [$p_e = 20$ MPa (—), p. = 80 MPa (- - -)], $R_{si}^0 = 5R_d^0$ [$p_e = 20$ MPa (— —), $p_e = 80$ MPa (– ···—)] and $R_{si}^0 = 2R_d^0$ [$p_e = 20$ MPa (– . – ·--), $p_e = 80$ MPa (····)]. All other initial conditions are those of Fig. 3 caption.

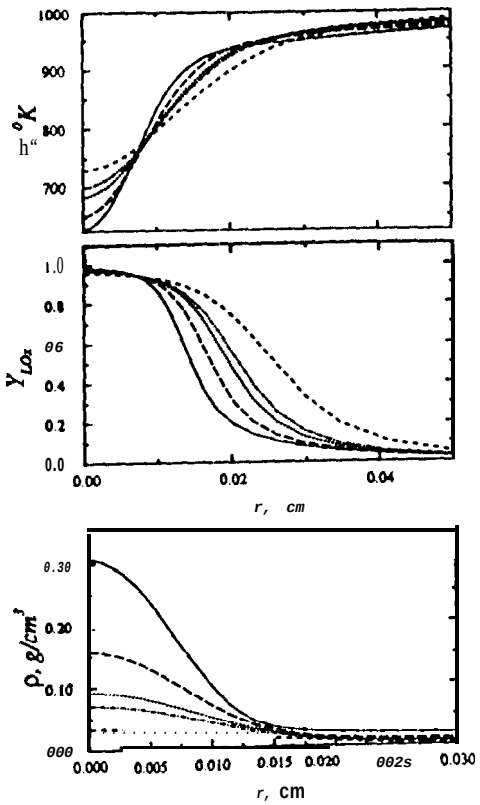

Fig. 6 Spatial variation of the isolated fluid drop temperate, oxygen mass fraction and density at 2×10^{-2} s for several pressures: 10 MPa (- - -), 20 MPa (– .- .-), 25 MPa (. . . ·),40 MPa (– --), 80 MPa (– . .–). other initial conditions are: R_d^0 = 50 X 10^{-4} cm, R_{si}^0 = 0.1 cm, $T_{d,b}^0 = 100$ K , $T_{si}^0 = 1000$ K.

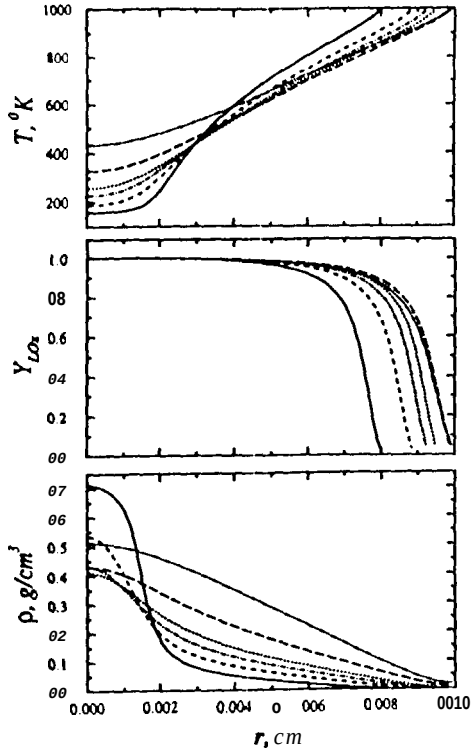

Fig. 7 Spatial variation of the cluster fluid drop temperature (a), oxygen mass fraction (b) and density (c) at 1X10-2 s for several pressures: 10 MPa (——-), 15 MPa (- - -), 20 MPa (– . – ·—),25 MPa (· . . .), 40 MPa (— —-), 80 MPa (--- ·--). Other initial conditions are those of Fig. 3 caption.